FLIGHT CONTROL OF A MULTIROTOR AERIAL VEHICLE USING A NONSINGULAR TERMINAL SLIDING MODE CONTROL

Arioberto Luciano da Silva Júnior

Davi Antônio dos Santos

ariobertoluciano@gmail.com

davists@ita.br

Instituto Tecnológico de Aeronáutica

Praça Marechal Eduardo Gomes, 50, Vila das Acácias, 12228-900, São José dos Campos, SP, Brazil

Abstract. *A multirotor aerial vehicle (MAV) is a highly nonlinear coupled system with uncertain parameters and subject to force and torque disturbances. The purpose of the present work is to design a flight control system for an autonomous quadrotor vehicle using a recent formulation of the sliding mode control (SMC) strategy, namely the nonsingular fast terminal sliding model control (NFTSMC), to track a desired trajectory. A hierarchical control structure is adopted by considering a time-scale separation between the translational and rotation dynamics. In this structure, the position control is realized by an outer slower loop, while the attitude control is carried out by an inner faster loop. For each loop, we first formulate a six-state dynamics model for the respective tracking error and then apply the NFTSMC strategy to steer it toward the origin. In particular, the tracking error of the rotational motion, the modified Rodrigues parameters are considered for representing the attitude error. Considering that the torque and force disturbances are bounded inside known sets, the adopted strategy leads to attitude and position control laws that are capable to globally track a desired trajectory with finite-time convergence and singularity avoidance. The proposed method is evaluated on extensive numerical simulations, showing its effectiveness as well as some of its properties.*

Keywords: *Multirotor aerial vehicle, Flight control, Terminal sliding mode control*

1 INTRODUCTION

In recent years, researchers from diverse areas have worked intensively in the development of multirotor unnamed aerial vehicles (UAV). These flying machines are capable of performing missions with minimum or no human intervention. Such interest can be explained by its capacity of hovering and to perform complex maneuvers. A lot of applications are appropriate for MAV such as surveillance and tactical awareness, topographic mapping, traffic monitoring, search and rescue of lost people, agricultural monitoring and others.

The flight control system is responsible for maneuverability and hovering capacity of MAV. In order to achieve these requirements, there are a plenty of methods for designing attitude and position controllers for MAVs, using different control strategies such as saturated-PD controllers (Santos et al., 2013), model predictive controllers (Prado and Santos, 2017), and adaptive controllers (Yan et al., 2014), just to cite a few examples. However, most of these techniques require an exact knowledge of the system dynamics. Whereas, the sliding mode control ensures robustness against the parametric uncertainties, the unmodeled dynamics, and the disturbances such as wind, turbulence of motors, etc. There are some works of SMC applied to tracking and regulation tasks for multirotor. A tradition sliding mode control was proposed in Silva and Santos (2014), which can guarantee the exponential convergence. In order to achieve the finite-time convergence, a terminal SMC was designed using a new switching surface in Xiong and Zheng (2014).

The present paper is concerned with the flight control system of multirotor helicopter UAVs. The main contribution is the design of the attitude and position laws using a recent nonsingular fast terminal sliding model control strategy. Which provides with some superior properties such as fast finite-time convergence, strong robustness and singularity avoidance. The remaining text is organized in the following sequence. Section 2 formally define the flight control problem for multirotor helicopter UAVs. Section 3 provides a solution to the main problem of the paper. This solution consists of two SMC controllers with using NFTSMC strategy to regulating the tracking error at origin. Section 4 evaluates the proposed method using computational simulations. Lastly, Section 5 presents the conclusions of the paper.

2 DYNAMIC MODELING

Consider the multirotor vehicle and the three Cartesian coordinate systems (CCS) illustrated in Fig. 1. The body CCS is denoted by $\mathcal{S}_B \triangleq \{\hat{x}_B, \hat{y}_B, \hat{z}_B\}$. It is attached to the vehicle's structure with the origin at its center of mass B. The reference CCS is denoted by $\mathcal{S}_{\bar{B}} \triangleq \{\hat{x}_{\bar{B}}, \hat{y}_{\bar{B}}, \hat{z}_{\bar{B}}\}$. It is defined by the attitude and position commands. The ground CCS is denoted by $\mathcal{S}_G \triangleq \{\hat{x}_G, \hat{y}_G, \hat{z}_G\}$. It is fixed on the ground at a known point O.

2.1 Rotor Dynamics and Efforts

Each rotor produces a thrust force f_i and a reaction torque τ_i on the airframe along the $\hat{z}_B$ axis. These efforts are modeled by $f_i = k_f\omega_i^2$ and $\tau_i = k_\tau\omega_i^2$, $i = 1, ..., 4$, where ω_i is the rotation speed of the ith rotor, k_f is the thrust force coefficient and k_τ is the reaction torque coefficient. Besides, the rotor dynamics can be modeled by the following first-order linear model

$$\dot{\omega}_i = -\frac{1}{\tau_\omega}\omega_i + \frac{k_\omega}{\tau_\omega}\bar{\omega}_i, \tag{1}$$

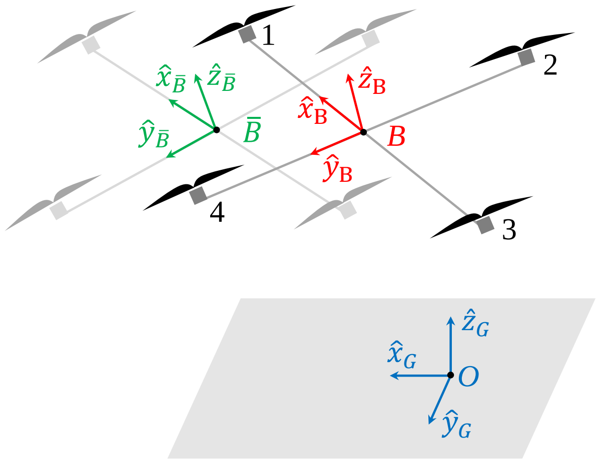

Figure 1: Cartesian coordinate systems.

where $\bar{\omega}_i$ is the rotation speed command of the ith rotor, k_ω is the speed coefficient and τ_ω is the rotor time constant.

Consider that the reaction torque τ_1 is positive, τ_2 is negative, τ_3 is positive, and so on. Therefore, the magnitude F^c of the resulting control force $\vec{\boldsymbol{F}}^c$ and the $\mathcal{S}_B$ representation of the resulting control torque $\vec{\boldsymbol{T}}^c$ are

$$\begin{bmatrix} F^c \\ \boldsymbol{T}^c_B \end{bmatrix} = \boldsymbol{\Gamma} \boldsymbol{f}, \tag{2}$$

where $\boldsymbol{f} \triangleq [\ f_1 \quad f_2 \quad f_3 \quad f_4\ ]^T$, l is the length of vehicle's arm, $k \triangleq k_\tau / k_f$ and

$$\boldsymbol{\Gamma} \triangleq \begin{bmatrix} 1 & 1 & 1 & 1 \\ 0 & -l & 0 & l \\ -l & 0 & l & 0 \\ k & -k & k & -k \end{bmatrix}. \tag{3}$$

2.2 Rotational Motion

Let $\boldsymbol{D} \triangleq \boldsymbol{D}^{B/G}$ and $\bar{\boldsymbol{D}} \triangleq \boldsymbol{D}^{\bar{B}/G}$ be the actual and the desired attitude expressed in direction cosine matrix (DCM), respectively. The attitude error expressed in terms of DCM is defined by $\tilde{\boldsymbol{D}} \triangleq \boldsymbol{D}\bar{\boldsymbol{D}}^T$. Moreover, denote the angular velocity vector of $\mathcal{S}_B$ with respect to $\mathcal{S}_G$ by $\vec{\boldsymbol{\Omega}}^{B/G}$, and its $\mathcal{S}_B$ representation by $\boldsymbol{\Omega}^{B/G}_B$. Using this previous notation, the true angular velocity is described by $\boldsymbol{\Omega} \triangleq \boldsymbol{\Omega}^{B/G}_B$, and $\bar{\boldsymbol{\Omega}} \triangleq \boldsymbol{\Omega}^{\bar{B}/G}_{\bar{B}}$ represents the desired angular velocity. Therefore, the angular velocity error is defined by $\tilde{\boldsymbol{\Omega}} \triangleq \boldsymbol{\Omega} - \tilde{\boldsymbol{D}}\bar{\boldsymbol{\Omega}}$.

In order to use a minimal parametrization, the modified Rodrigues parameters (MRP) will be use to represent the attitude error kinematics (Younes et al., 2014)

$$\dot{\tilde{\boldsymbol{p}}} = -\frac{1}{2}([\boldsymbol{\Omega}\times] + [\bar{\boldsymbol{\Omega}}\times])\tilde{\boldsymbol{p}} + \frac{1}{4}(1 - \tilde{\boldsymbol{p}}^T\tilde{\boldsymbol{p}})(\boldsymbol{\Omega} - \bar{\boldsymbol{\Omega}}) + \frac{1}{2}[(\boldsymbol{\Omega} - \bar{\boldsymbol{\Omega}})^T\tilde{\boldsymbol{p}}]\tilde{\boldsymbol{p}}, \tag{4}$$

where $\tilde{\boldsymbol{p}}$ is the MRPs error and $[\boldsymbol{v}\times]$ is the skew-symmetric matrix of a vector $\boldsymbol{v} = \begin{bmatrix} v_1 & v_2 & v_3 \end{bmatrix}^T$.

Using the Newton-Euler formulation, the model of attitude dynamics of the quadrotor vehicle is given by

$$\dot{\tilde{\boldsymbol{\Omega}}} = -\boldsymbol{J}^{-1}[(\boldsymbol{J}\boldsymbol{\Omega})\times]\boldsymbol{\Omega} + \boldsymbol{J}^{-1}\boldsymbol{T}_B^c + \boldsymbol{J}^{-1}\boldsymbol{T}_B^d - \dot{\tilde{\boldsymbol{D}}}\bar{\boldsymbol{\Omega}} - \tilde{\boldsymbol{D}}\dot{\bar{\boldsymbol{\Omega}}}, \tag{5}$$

where $\boldsymbol{J}$ is the body inertia matrix and $\boldsymbol{T}_B^d$ is the disturbance torque $\vec{\boldsymbol{T}}^d$ represented in $\mathcal{S}_B$.

2.3 Translational Motion

Denote by $\vec{\boldsymbol{r}}^{B/G}$ and $\vec{\boldsymbol{v}}^{B/G}$ the position and velocity vectors of $\mathcal{S}_B$ with respect to $\mathcal{S}_G$, respectively. The representation of these vectors in reference CCS are $\boldsymbol{r}_G^{B/G}$ and $\boldsymbol{v}_G^{B/G}$. Besides, let $\bar{\boldsymbol{r}} \triangleq \boldsymbol{r}_G^{\bar{B}/G}$ be the desired position, and $\bar{\boldsymbol{v}} \triangleq \boldsymbol{v}_G^{\bar{B}/G}$ be the desired velocity. Therefore, the position and velocity errors are defined by $\tilde{\boldsymbol{r}} \triangleq \bar{\boldsymbol{r}} - \boldsymbol{r}$ and $\tilde{\boldsymbol{v}} \triangleq \bar{\boldsymbol{v}} - \boldsymbol{v}$, respectively.

According to second Newton's law, the translational error dynamics is

$$\ddot{\tilde{\boldsymbol{r}}} = \ddot{\bar{\boldsymbol{r}}} - \boldsymbol{g}_G - \frac{1}{m}\boldsymbol{F}_G^c - \frac{1}{m}\boldsymbol{F}_G^d, \tag{6}$$

where m is the vehicle's mass, $\boldsymbol{F}_G^d$ is the disturbance torque $\vec{\boldsymbol{F}}^d$ in $\mathcal{S}_G$, and the gravitational acceleration vector in $\mathcal{S}_G$ is $\boldsymbol{g}_G = \begin{bmatrix} 0 & 0 & -g \end{bmatrix}^T$.

3 FLIGHT CONTROL SYSTEM

The flight control of a MAV is divided into two parts by considering a time-scale separation between the translational and rotation dynamics (Bertrand et al., 2011). The structure adopted is an inner faster loop to control attitude and an outer slower loop to control position, accordingly the Fig. 2.

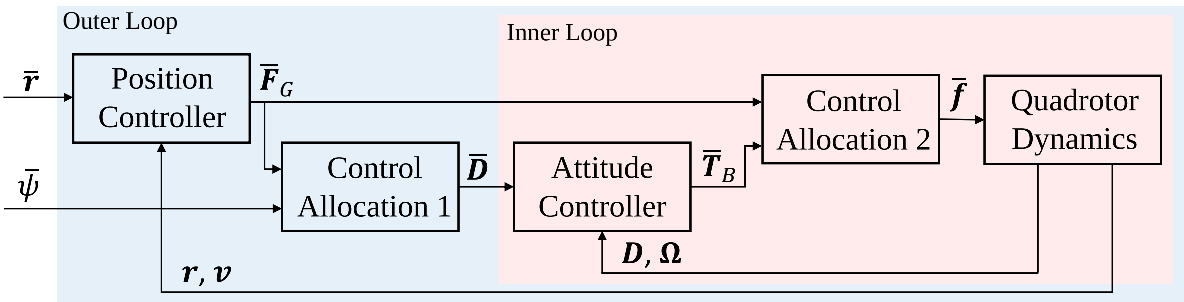

Figure 2: The structure of quadrotor flight control.

3.1 Attitude Controller

Consider that the command of torque $\bar{\boldsymbol{T}}_B$ is equal to resulting control torque $\boldsymbol{T}_B^c$, and the desired angular velocity $\bar{\boldsymbol{\Omega}}$ is zero. From Eq. 4 and 5, the attitude design model is

$$\begin{cases} \dot{\tilde{\boldsymbol{p}}} = \boldsymbol{F}_1(\tilde{\boldsymbol{p}}, \tilde{\boldsymbol{\Omega}}) \\ \dot{\tilde{\boldsymbol{\Omega}}} = \boldsymbol{F}_2(\tilde{\boldsymbol{\Omega}}) + \boldsymbol{J}^{-1}\bar{\boldsymbol{T}}_B + \boldsymbol{J}^{-1}\boldsymbol{T}_B^d \end{cases}, \tag{7}$$

where

$$\begin{cases} \boldsymbol{F}_1(\tilde{\boldsymbol{p}}, \tilde{\boldsymbol{\Omega}}) \triangleq \frac{1}{4}[-2[\tilde{\boldsymbol{\Omega}}\times]\tilde{\boldsymbol{p}} + (1 - \tilde{\boldsymbol{p}}^T\tilde{\boldsymbol{p}})\tilde{\boldsymbol{\Omega}}] + \frac{1}{2}(\tilde{\boldsymbol{\Omega}}^T\tilde{\boldsymbol{p}})\tilde{\boldsymbol{p}} \\ \boldsymbol{F}_2(\tilde{\boldsymbol{\Omega}}) \triangleq -\boldsymbol{J}^{-1}[(\boldsymbol{J}\tilde{\boldsymbol{\Omega}})\times]\tilde{\boldsymbol{\Omega}} \end{cases}. \tag{8}$$

Let be the three-dimensional time-varying sliding surface for attitude:

$$\boldsymbol{S}_a = \tilde{\boldsymbol{p}} + \boldsymbol{\Lambda}_1 \text{sign}^{\boldsymbol{\Gamma}_1}(\tilde{\boldsymbol{p}}) + \boldsymbol{\Lambda}_2 \text{sign}^{\boldsymbol{\Gamma}_2}(\dot{\tilde{\boldsymbol{p}}}), \tag{9}$$

where the involved matrices are $\boldsymbol{\Lambda}_1 = \text{diag}(\lambda_{11}, \lambda_{12}, \lambda_{13})$, $\boldsymbol{\Gamma}_1 = \text{diag}(\gamma_{11}, \gamma_{12}, \gamma_{13})$, $\boldsymbol{\Lambda}_2 = \text{diag}(\lambda_{21}, \lambda_{22}, \lambda_{23})$, and $\boldsymbol{\Gamma}_2 = \text{diag}(\gamma_{21}, \gamma_{22}, \gamma_{23})$, with $\lambda_{1i} > 0$, $\lambda_{2i} > 0$, $\gamma_{1i} > \gamma_{2i}$, $1 < \gamma_{2i} < 2$, for $i = 1, 2, 3$. Besides, $\text{sign}^{\boldsymbol{\Gamma}_1}(\tilde{\boldsymbol{p}})$ is a vector defined as $\text{sign}^{\boldsymbol{\Gamma}_1}\tilde{\boldsymbol{p}} \triangleq \text{diag}[\text{sign}(\tilde{\boldsymbol{p}})] \cdot |\tilde{\boldsymbol{p}}|^{\boldsymbol{\Gamma}_1} = [\ \text{sign}(\tilde{p}_1)|\tilde{p}_1|^{\gamma_{11}} \quad \text{sign}(\tilde{p}_2)|\tilde{p}_2|^{\gamma_{12}} \quad \text{sign}(\tilde{p}_3)|\tilde{p}_3|^{\gamma_{13}}\ ]^T$, and $\text{sign}^{\boldsymbol{\Gamma}_2}(\dot{\tilde{\boldsymbol{p}}})$ is defined similarly.

Under assumption of the disturbance torque $\boldsymbol{T}_B^d$ is bounded by a constant t_d, the attitude control law using NFTSMC method is given by

$$\begin{aligned} \bar{\boldsymbol{T}}_B = &- \boldsymbol{J}\left(\frac{\partial \boldsymbol{F}_1}{\partial \tilde{\boldsymbol{\Omega}}}\right)^{-1}\Bigg[c_2\boldsymbol{S}_a + \left(\left\|\frac{\partial \boldsymbol{F}_1}{\partial \tilde{\boldsymbol{\Omega}}}\right\|\|\boldsymbol{J}^{-1}\|t_d + c_1\right)\frac{\boldsymbol{S}_a}{\|\boldsymbol{S}_a\| + \delta_1} + \frac{\partial \boldsymbol{F}_1}{\partial \tilde{\boldsymbol{p}}}\boldsymbol{F}_1 \\ &+ \frac{\partial \boldsymbol{F}_1}{\partial \tilde{\boldsymbol{\Omega}}}\boldsymbol{F}_2 + {\boldsymbol{\Lambda}_2}^{-1}{\boldsymbol{\Gamma}_2}^{-1}(\boldsymbol{I}_3 + \boldsymbol{\Lambda}_1\boldsymbol{\Gamma}_1\text{diag}(|\tilde{\boldsymbol{p}}|^{\boldsymbol{\Gamma}_1 - \boldsymbol{I}_3}))\text{sign}^{2\boldsymbol{I}_3 - \boldsymbol{\Gamma}_2}(\dot{\tilde{\boldsymbol{p}}})\Bigg], \end{aligned} \tag{10}$$

where $c_1 > 0$, $c_2 > 0$, $\delta_1 \geq 0$ is a small constant, and $\boldsymbol{I}_3$ is the three-dimensional unit matrix. This attitude controller Eq. 10 leads a finite-time reaching phase to sliding surface Eq. 9. Once the manifold is reached, it ensures a sliding mode phase to origin with finite-time convergence and singularity avoidance. The proof is similar it to found in Yang and Yang (2010).

3.2 Position Controller

Consider that the command of force $\bar{\boldsymbol{F}}_G$ is equal to the resulting control force $\boldsymbol{F}_G^c$, and the desired acceleration $\ddot{\bar{\boldsymbol{r}}}$ is zero. From Eq. (6), the position design model is

$$\begin{cases} \dot{\tilde{\boldsymbol{r}}} = \tilde{\boldsymbol{v}} \\ \dot{\tilde{\boldsymbol{v}}} = -\boldsymbol{g}_R - \frac{1}{m}\bar{\boldsymbol{F}}_G - \frac{1}{m}\boldsymbol{F}_G^d \end{cases}. \tag{11}$$

Let be the three-dimensional time-varying sliding surface for position:

$$\boldsymbol{S}_p = \tilde{\boldsymbol{r}} + \boldsymbol{\Lambda}_3 \text{sign}^{\boldsymbol{\Gamma}_3}(\tilde{\boldsymbol{r}}) + \boldsymbol{\Lambda}_4 \text{sign}^{\boldsymbol{\Gamma}_4}(\dot{\tilde{\boldsymbol{r}}}), \tag{12}$$

where the involved matrices are $\boldsymbol{\Lambda}_3 = \text{diag}(\lambda_{31}, \lambda_{32}, \lambda_{33})$, $\boldsymbol{\Gamma}_3 = \text{diag}(\gamma_{31}, \gamma_{32}, \gamma_{33})$, $\boldsymbol{\Lambda}_4 = \text{diag}(\lambda_{41}, \lambda_{42}, \lambda_{43})$, and $\boldsymbol{\Gamma}_4 = \text{diag}(\gamma_{41}, \gamma_{42}, \gamma_{43})$, with $\lambda_{3i} > 0$, $\lambda_{4i} > 0$, $\gamma_{3i} > \gamma_{4i}$, $1 < \gamma_{4i} < 2$, for $i = 1, 2, 3$.

Under assumption of the disturbance force $\boldsymbol{F}_G^d$ is bounded by a constant f_d, the position control law using NFTSMC method is given by

$$\begin{aligned} \bar{\boldsymbol{F}}_G = m\Bigg[&c_4\boldsymbol{S}_p + \left(\frac{f_d}{m} + c_3\right)\frac{\boldsymbol{S}_p}{\|\boldsymbol{S}_p\| + \delta_2} - \boldsymbol{g}_G + \boldsymbol{\Lambda}_4^{-1}\boldsymbol{\Gamma}_4^{-1}(\boldsymbol{I}_3 \\ &+ \boldsymbol{\Lambda}_3\boldsymbol{\Gamma}_3\text{diag}(|\tilde{\boldsymbol{r}}|^{\boldsymbol{\Gamma}_3 - \boldsymbol{I}_3}))\text{sign}^{2\boldsymbol{I}_3 - \boldsymbol{\Gamma}_4}(\dot{\tilde{\boldsymbol{r}}})\Bigg], \end{aligned} \tag{13}$$

where $c_3 > 0$, $c_4 > 0$, and $\delta_2 \geq 0$ is a small constant. As the attitude controller, the stability and the time-finite convergence proofs are similar to it found in Yang and Yang (2010).

3.3 Control Allocation

Control Allocation 1

Let $\bar{\psi}$ be an arbitrary command for heading angle. The attitude command is given by

$$\bar{\boldsymbol{D}} = \boldsymbol{D}_3(\bar{\psi})\boldsymbol{D}_{\bar{\boldsymbol{a}}}(\bar{\phi}) \tag{14}$$

where $\boldsymbol{D}_3(\bar{\psi})$ is the elementary rotation matrix about the z-axis, through an angle $\bar{\psi}$. Besides, $\boldsymbol{D}_{\bar{\boldsymbol{a}}}(\bar{\phi}) = \cos\bar{\phi}\boldsymbol{I}_3 + (1-\cos\bar{\phi})\bar{\boldsymbol{a}}\bar{\boldsymbol{a}}^T - \sin\bar{\phi}[\bar{\boldsymbol{a}}\times]$, where $\bar{\boldsymbol{a}} = [\boldsymbol{e}_3\times]\bar{\boldsymbol{F}}_G/\bar{F}$ and $\bar{\phi} = \cos^{-1}(\bar{F}_z/\bar{F})$, with $\boldsymbol{e}_3 = [\ 0 \quad 0 \quad 1\ ]^T$ and $\bar{F}_z$ is the component of $\bar{\boldsymbol{F}}_G$ along the $\hat{z}_G$ axis.

Control Allocation 2

From the magnitude of force command $\bar{F}$ and the $\mathcal{S}_B$ representation of the torque command $\bar{\boldsymbol{T}}_B$ can be determined the force commands for each rotor. Using the Equation (2), the individuals thrust commands are given by

$$\bar{\boldsymbol{f}} = \boldsymbol{\Gamma}^{-1}\begin{bmatrix} \bar{F} \\ \bar{\boldsymbol{T}}_B \end{bmatrix}, \tag{15}$$

where $\bar{\boldsymbol{f}} \triangleq [\ \bar{f}_1 \quad \bar{f}_2 \quad \bar{f}_3 \quad \bar{f}_4\ ]^T$.

4 COMPUTATIONAL SIMULATION

The system was simulated using the Runge-Kutta method with an integration step of $T = 0.01$ s. The parameters of the plant are: a mass of $m = 0.7$ kg, an inertia matrix of $\boldsymbol{J} = \mathrm{diag}(0.02, 0.02, 0.03)$ kgm^2, an arm length of $l = 0.2$ m, a force coefficient of $k_f = 3.13\times10^{-5}$ $\mathrm{N/(rad/s)^2}$, a torque coefficient of $k_\tau = 7.5\times10^{-7}$ $\mathrm{Nm/(rad/s)^2}$, a speed coefficient of $k_w = 1$, and a time constant of $\tau_w = 0.1$ s. Also, the gravitational acceleration is $g = 9.81$ $\mathrm{m/s^2}$. The attitude controller parameters are: $\boldsymbol{\Lambda}_1 = 10\boldsymbol{I}_3$, $\boldsymbol{\Gamma}_1 = 1.1\boldsymbol{I}_3$, $\boldsymbol{\Lambda}_2 = 5\boldsymbol{I}_3$, $\boldsymbol{\Gamma}_2 = 1.2\boldsymbol{I}_3$, $c_1 = 1$, $c_2 = 1$, $\delta_1 = 0.1$, and $t_d = 0.1$ Nm. The position controller parameters are: $\boldsymbol{\Lambda}_3 = 10\boldsymbol{I}_3$, $\boldsymbol{\Gamma}_3 = 1.01\boldsymbol{I}_3$, $\boldsymbol{\Lambda}_4 = \boldsymbol{I}_3$, $\boldsymbol{\Gamma}_4 = 1.02\boldsymbol{I}_3$, $c_3 = 1$, $c_4 = 1$, $\delta_2 = 0.1$, and $f_d = 0.5$ N.

In order to evaluate the proposed control method, the quadrotor was commanded to follow the waypoints trajectory. In this path, the waypoints are connected by straight lines of 3 m, with constant desired speed of $\bar{v} = 0.5$ m/s and the heading angle command is $\bar{\psi} = 0$ rad. The Gaussian disturbances force and torque with zero means and covariances $\boldsymbol{Q}_f = 10^{-2}\boldsymbol{I}_3$ N^2 and $\boldsymbol{Q}_\tau = 10^{-4}\boldsymbol{I}_3$ $(\mathrm{Nm})^2$, respectively, are taken into account in this test. The results are shown in Fig. 3-5.

Figure 3 shows the actual position and the corresponding position command. At the beginning of flight, it occurred a short delay because the vehicle was stopped and the trajectory command had a constant desired speed of $\bar{v} = 0.5$ m/s. Besides, for each waypoint there are low overshoots less than 0.2 m.

Figure 4 shows the performance of the attitude control loop. In order to do the maneuvers, the attitude pitch and roll commands oscillate at the waypoints. For these points, the corresponding true attitude angles follow them with an apparently slow and attenuated response.

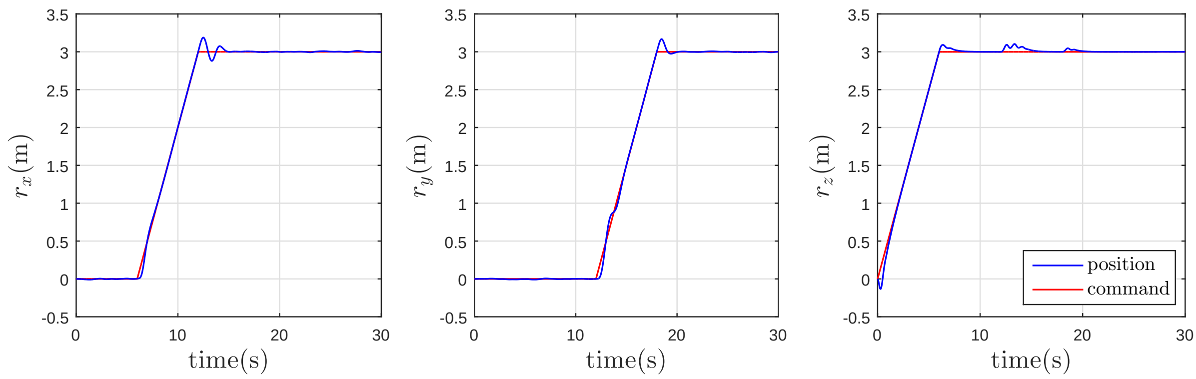

Figure 3: Performance of the position control.

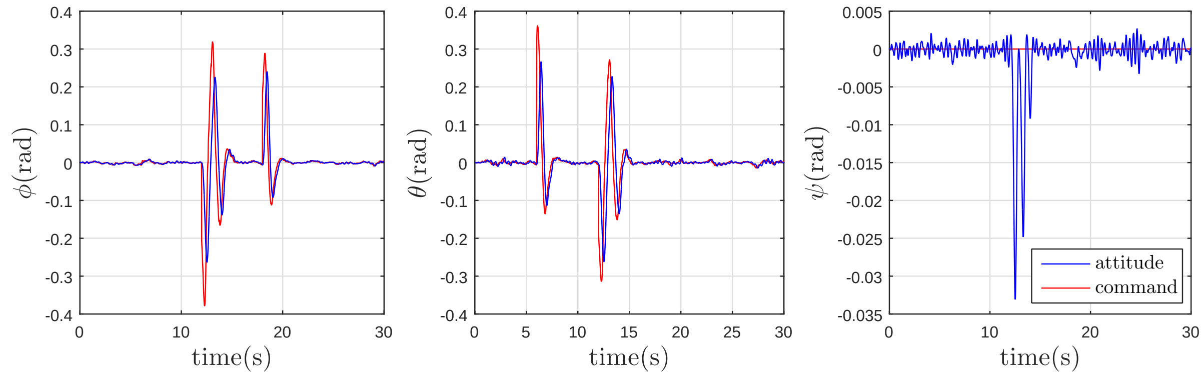

Figure 4: Performance of the attitude control.

Finally, Fig. 5 (a) shows the components of the torque command $\bar{\boldsymbol{T}}_B$ generated by the attitude controller and Fig. 5 (b) presents the force magnitude command $\bar{F}$ computed by the position controller. The $\hat{x}_B$ and $\hat{y}_B$ components of the torque command $\bar{\boldsymbol{T}}_B$ oscillate at the waypoints to reach the desired roll and pitch angles. The force command $\bar{F}$ has maximum at the beginning part of the trajectory where the vehicle is command to ascend. After the transients caused by the maneuvers at the waypoints, $\bar{F}$ seems to converge and stay around 6.867 N, which is equivalent to the total weigh of the vehicle. Besides, during all simulation, the command force and torque try to minimize the presence of Gaussian disturbances.

5 CONCLUSION

This work presented a flight control system for an autonomous quadrotor vehicle using a NFTSMC strategy. The numerical simulation results shown the effectiveness of the proposed flight control method. For a waypoints trajectory and it subject to high disturbance force and torque, the vehicle was able to track very well the trajectory command. For a future work, will be considerate a multirotor subject to actuator saturation. This approach is more realist, which possibility the application in real activities.

ACKNOWLEDGEMENTS

The authors would like to thank CAPES, CNPq (grant 475251/2013-0) and FAPESP (grant 2015/04393-2) for the support in the current research projects of the Laboratório de Robótica

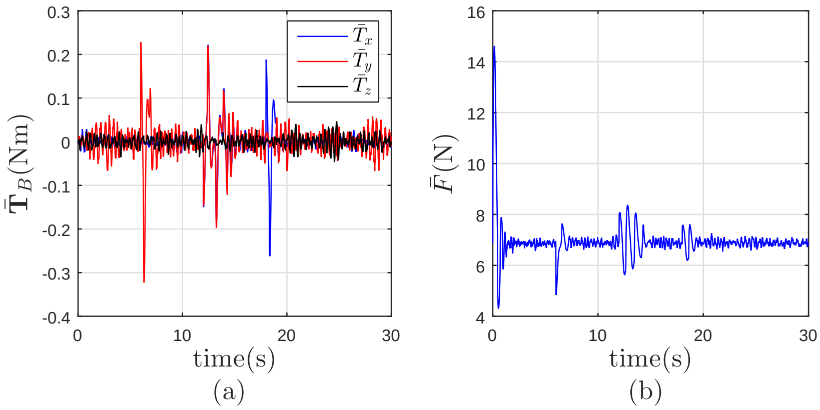

Figure 5: (a) Torque command. (b) Force magnitude command.

Aérea of the Instituto Tecnológico de Aeronáutica.

REFERENCES

Bertrand, S., Guénard, N., Hamel, T., Piet-Lahanier, H., & Eck, L., 2011. A hierarchical controller for miniature VTOL UAVs: Design and stability analysis using singular perturbation theory. *Control Engineering Practice*, vol. 19, n. 10, pp. 1099-1108.

Prado, I. A. A., & Santos, D. A., 2017. A Model Predictive Guidance Strategy for a Multirotor Aerial Vehicle. *Journal of Aerospace Technology and Management*, vol. 9, n. 1, pp. 116-128.

Santos, D. A., Saotome, O., & Cela, A., 2013. Trajectory Control of Multirotor Helicopters With Thrust Vector Constraints. In Platanias, *21st Mediterranean Conference on Control and Automation* (MED), pp. 375-379.

Silva, J. A. B. G., & Santos, D. A., 2016. Sliding mode control applied to waypoint-based guidance of multirotor aerial vehicles. In Vitória, *Congresso Brasileiro Automática* (CBA).

Xiong, J.-J., & Zheng, E.-H., 2014. Position and attitude tracking control for a quadrotor UAV. *ISA Transactions*, vol. 53, n. 3, pp. 725-731.

Yan, J., Santos, D. A., & Bernstein, D. S., 2014. Adaptive control with convex saturation constraints. *IET Control Theory and Applications*, vol. 8, n. 12, pp. 1096-1104.

Yang, L., & Yang, J., 2010. Nonsingular fast terminal sliding-mode control for nonlinear dynamical systems. *International Journal of Robust and Nonlinear Control*, vol. 21, n. 16, pp. 1865-1879.

Younes, A. B., Mortari, D., Tumer, J. D., & Junkins, J. L., 2014. Attitude error kinematics. *Journal of Guidance, Control and Dynamics*, vol. 37, n. 1, pp. 330-336.